BMC Chemistry

https://doi.org/10.1186/s13065-025-01697-7

Article in Press

Synthesis and thermo-oxidative kinetic analysis of cellulose microfibers from palm leaves using ammonia fiber expansion

Received: 8 September 2025

Accepted: 26 November 2025

Published online: 02 December 2025

Cite this article as: Badran I., Yousef D., Manasrah A.D. *et al.* Synthesis and thermo-oxidative kinetic analysis of cellulose microfibers from palm leaves using ammonia fiber expansion. *BMC Chemistry* (2025). https://doi.org/10.1186/s13065-025-01697-7

Ismail Badran, Duha Yousef, Abdallah D. Manasrah, Derar Al-Smadi, Kotaybah Hashlamoun & Nashaat N. Nassar

Synthesis and Thermo-Oxidative Kinetic Analysis of Cellulose Microfibers from Palm Leaves Using Ammonia Fiber Expansion

Ismail Badran,*[a] Duha Yousef,[a] Abdallah D. Manasrah[b&c], Derar Al-Smadi,[a]
Kotaybah Hashlamoun[b] Nashaat N. Nassar[b]

[a] Department of Chemistry, Faculty of Sciences, An-Najah National University, Nablus, Palestine

[b] Department of Chemical and Petroleum Engineering, University of Calgary, 2500 University Street NW, Calgary, Alberta, Canada T2N 1N4.

[c] Carbon OxyTech Inc., 3655 36 St NW, Calgary, Alberta, Canada T2L 1Y8

*Corresponding Author: Ismail Badran, Tel.: +970 598142621, E-mail: i.badran@najah.edu

Keywords

Ammonia Fiber Expansion, Cellulose Microfibers, Agricultural Waste, Isoconversional Kinetics, Sustainable Biomass Conversion

Abstract

Global urbanization is driving high volumes of agricultural and food waste, creating an urgent need for sustainable and effective technologies to convert biomass into valuable products. This study explores the conversion of palm waste into cellulose microfibers (CMF) using Ammonia Fiber Expansion (AFEX) followed by acid hydrolysis, with a focus on structural characterization, thermal stability, and reaction kinetics compared to raw material.

The resulting CMF exhibited elongated, uniform fibers with smooth surfaces, with lengths of 0.1–3.0 mm, and diameters of 5–20 µm. X-ray analysis revealed a significant increase in the carbon/oxygen ratio, from 1.8 ± 0.2 in raw palm leaves to 2.7 ± 0.3 in CMF, indicating enhanced carbon content due to dehydration and reduction of carbonyl groups. FTIR spectra confirmed effective removal of lignin and hemicellulose after treatment, further supporting this chemical transformation.

Thermal analysis demonstrated that CMF possesses higher heat content than raw leaves, suggesting its potential for energy-related applications. TGA showed that CMF decomposes at slightly higher temperatures, indicating improved thermal stability. Isoconversional kinetic analysis using the Vyazovkin Nonlinear (NLN) and Kissinger-Akahira-Sunose (KAS) methods revealed variable effective activation energies (E_α), consistent with a complex degradation mechanism. Overall, CMF displayed lower E_α values than raw biomass, especially at early and mid-reaction stages.

Kinetic modeling at 50% conversion showed a markedly higher pre-exponential factor (A_α) for raw leaves (2.8×10^{13} s^{-1}) compared to CMF (7.4×10^{9} s^{-1}), reflecting structural alterations from treatment. Both raw and CMF samples exhibited negative activation entropy ($\Delta S^{\neq}$) values of –237.7 and –240.3 $J\,mol^{-1}\,K^{-1}$, respectively, suggesting greater molecular order in activated complexes. The enthalpy of activation ($\Delta H^{\neq}$) was 149.7 ± 3.9 $kJ\,mol^{-1}$ for raw leaves versus 120.4 ± 3.9 $kJ\,mol^{-1}$ for CMF, Gibbs free energy of activation ($\Delta G^{\neq}$) was slightly higher for raw leaves (297.0 ± 3.9 $kJ\,mol^{-1}$) compared to CMF (269.4 ± 3.9 $kJ\,mol^{-1}$), primarily due to differences in $\Delta H^{\neq}$. These kinetic parameters are crucial for any future implementation of palm leaves conversion into CMF at the industrial scale.

Introduction

The accelerating pace of urbanization, driven by population growth and socioeconomic changes, has placed immense pressure on global food production and supply chains. This escalation results in the accumulation of vast quantities of agricultural waste, compounded by social habits such as the disposal of food leftovers. Although much of this waste is inherently biodegradable, the 4R concept (reduce, reuse, recycle, and repurpose) necessitates the development of innovative and scalable technologies that transform agricultural waste into valuable resources [1-3].

Despite efforts made by many countries to manage and recycle agricultural waste, open burning remains the most dominant method of disposal, particularly in densely populated areas such as China, India, and Africa, as well as in many other nations [4, 5]. Open burning is a significant contributor to air pollution, releasing hazardous pollutants including greenhouse gases (GHGs), particulate matter (PM), and various toxic chemicals [6, 7].

Among various sources of agricultural waste, palm trees are considered a major contributor due to their extensive cultivation and their importance in palm oil production. According to the Food and Agriculture Organization (FAO), there are over 100 million date palm trees worldwide, producing more than 10 million metric tons of dates annually (as of 2024) [8]. The Middle Eastern countries contribute between 60 and 70% of the global date production, with Egypt, Saudi Arabia, and Iraq being the leading producers [8, 9]. With this in mind, palm cultivation generates massive amounts of waste, including fruit bunches, trunks, kernel shells, leaves, and husks. These materials, which are often discarded or burned, contribute significantly to environmental pollution [9, 10]. This motivated us to explore the conversion of palm waste into valuable materials, particularly microcellulose, through an innovative technology based on Ammonia Fiber Expansion (AFEX).

Since the time of Egyptian papyri, cellulose-based products have played a central role in the recording and transmission of knowledge [11]. One of these products, microcellulose, is a flexible, low-cost, biopolymer that is both biodegradable and non-hazardous. Microcellulose occurs in different shapes and has substantial applications in high-performance composites and other advanced applications. Microcellulose exists in different polymorphs, including cellulose nanocrystals (CNC) and cellulose microfibers (CMF), each with distinct structural characteristics and properties[12-15]. CNC can be described as crystalline nanoparticles with a highly ordered structure, while CMF are longer, more flexible, and entangled fibers.

One significant advantage of microcellulose materials is that they can be easily functionalized to enhance their properties. This can be achieved by modifying or adding functional groups to their surfaces using various techniques. Chemical modification of CNC and CMF improves their stability under thermal, chemical, and mechanical stress. Functionalized microcellulose materials find applications in drug delivery, wound healing,

tissue engineering, and energy storage in supercapacitors and batteries [16-19]. Additionally, microcellulose plays important roles in biodegradable packaging, composites, water filtration and purification products, cosmetic and personal care items, and environmental remediation [12-14].

While several technologies exist for producing microcellulose from agricultural waste, such as acid hydrolysis, catalytic pyrolysis, and enzymatic treatments, Ammonia Fiber Expansion (AFEX) offers distinct advantages [20]. AFEX, also known as ammonia steam explosion [21], is a novel pre-treatment method that utilizes ammonia to break down the lignocellulosic structure found in leaves structures (such as palm leaves in this study), enhancing their reactivity for subsequent steps (e.g., acid hydrolysis) [22, 23].

The term "expansion" refers to the critical step in AFEX, which involves the sudden release of pressure at the end of the reaction. In a typical AFEX treatment, the biomass is mixed with ammonia in a 1:3 ratio under high pressure (between 7 and 10 atm). As the mixture is heated, ammonia vapor increases the internal pressure to 10–20 atm, depending on the temperature. At the end of the process, pressure is quickly released by opening the vent valve, creating an explosive discharge that breaks down lignocellulosic, forming nanocrystals or microfibers. Additionally, AFEX is advantageous because it requires simple washing steps, thus reducing waste generation and processing costs [24, 25].

In this context, Thermogravimetric Analysis (TGA) and Differential Scanning Calorimetry (DSC) play a crucial role in revealing the transformations that raw materials undergo during treatment to produce the final product; in this case, CMF [20, 26-28]. These techniques are essential for tracking thermal stability and decomposition behavior. Moreover, isoconversional methods applied to TGA data allow for the determination of effective activation energies, which are critical for assessing thermal decomposition and understanding its kinetics [27, 29-31]. DSC can also be used to evaluate the thermal content of materials, as it directly quantifies the heat released or absorbed during the process, enabling accurate measurement of reaction enthalpies [27, 32].

The main goal of this study is to convert palm leaves into CMF using AFEX followed by acid hydrolysis. As the findings of the study indicate, the process resulted in the production of high-quality CMF. The formed CMF were characterized by FTIR and SEM coupled to EDX. The study also aims to evaluate the thermal stability and heat content of the produced CMF in comparison to the virgin materials. This is accomplished using TGA and DSC. The reaction kinetics were analyzed using advanced isoconversional kinetic methods, and a reaction model was developed to evaluate the pre-exponential factor (A) and the kinetic triplet ($\Delta H^{\ddagger}$, $\Delta S^{\ddagger}$, and $\Delta G^{\ddagger}$).

Experimental

Materials and Instruments

Palm leaves(*Phoenix dactylifera* - *Palmae*) were collected under authorization (see Ethics approval and consent to participate section) from

a local farm in the Jericho region, Palestine. The plants were identified by a pharmacognosist Prof. Nidal Jaradat and voucher specimens were deposited at the Natural Products Laboratory of the Faculty of Medicine and Health Sciences at An-Najah National University and kept under the herbarium voucher specimen number: Pharm-PCT-1842 [33, 34]. Ammonia solution (NH_4OH, 25%) was purchased from Riedel-de Haën (Seelze, Germany). Sodium hydroxide (NaOH, ≥97%), hydrogen peroxide (H_2O_2, 30%), and hydrochloric acid (HCl, 37%) were obtained from Sigma-Aldrich (St. Louis, Missouri, USA). Sodium hypochlorite (NaOCl, 10–15%) was supplied by Alfa Aesar (Haverhill, Massachusetts, USA). Milli-Q purified water was used throughout the experiments.

All solid samples in this study were weighed using MRC analytical balance ASB-310-C2-V2 (MRC). Solution pH was recorded by JENWAY 3510 pH meter (Cole-Parmer, USA). Infrared spectra were collected using a Fourier-transform infrared spectrometer (Thermo Scientific Nicolet iS5 FT-IR, Waltham, Massachusetts, USA). A stainless-steel reactor (1.0-L) equipped with a heating mantle (BMD 300, Buchiglasuster, Uster, Switzerland) was used for the AFEX experiments.

The TGA/DSC experiments were performed using a simultaneous thermal analyzer (SDT 650 TA Instruments, Waters LLC, New Castle, USA). In such analysis, the relative weight of the materials and the heat flow were measured simultaneously while raising the temperature. Each TGA run was performed by loading a small sample of each material into an open alumina crucible. The sample size was kept to a minimum (□5 mg) to avoid diffusion and mass transfer limitations [35, 36]. The sample was then heated to a temperature of 800 °C under continuous air purging at a rate of 100 mL min^{-1}. Various heating rates were performed (10, 15, 20, and 25 °C min^{-1}) for each sample in discrete runs. Both the mass change and heat flow were measured and recorded simultaneously during the run.

The morphological textures of the materials were examined using a Scanning Electron Microscope (SEM) of Phenom ProX (ThermoFisher Scientific, USA) equipped with an energy dispersive X-ray (EDX) analyzer. A specimen of each sample was initially sputtered with a carbon nanolayer and then loaded onto the instrument separately. Thereafter, a beam of energetic electrons (10–15 kV) was focused on the held sample, generating SEM images. Surface elemental analysis of the materials was performed using the SEM instrument in Energy-Dispersive X-ray (EDX) mode.

AFEX Experiments

The synthesis procedure of the CMF is shown in Fig. 1. The raw palm leaves were first dried in an oven at 60 °C for 24 h to remove water content. Using a crusher, the dried palm leaves were milled into granules ranging from 1 to 10 mm in size. For the AFEX reaction, the powdered raw palm leaves were placed in a 1.0-L stainless-steel high-pressure reactor. The biomass-to-ammonia ratio was maintained at approximately 1:3 (w/w). Approximately 15 grams of the palm leaves powder were weighed, and 100 mL of distilled water along with 200 mL of 25% NH_4OH were added to the reactor vessel. The reactor lid was securely fastened, and the entire reactor assembly was placed in a heating mantle.

The reactor was heated to temperatures ranging from 80 to 90 °C, and the pressure (due to ammonia gas) required to keep ammonia in its liquid state during the treatment ranged between 7 and 10 atm. These conditions were maintained for 2 h. The temperature and pressure were carefully controlled and monitored during the reaction. After the treatment, the mixture was gradually cooled to around 30 °C. Then, the reactor was opened to relieve the pressure. As mentioned earlier in the introduction, this is a critical step that allows the biomass fibers to expand, increase their surface area, and become more reactive for subsequent steps.

The treated palm leaves powder was then washed thoroughly with DW to remove residual ammonia. The washed palm leaves powder was placed on trays and dried in an oven at a low temperature (40-60 °C) until their moisture content was reduced to less than 10%. The percent yield for this step was ~ 45% (Fig. 1), in agreement with previous studies [18, 37, 38].

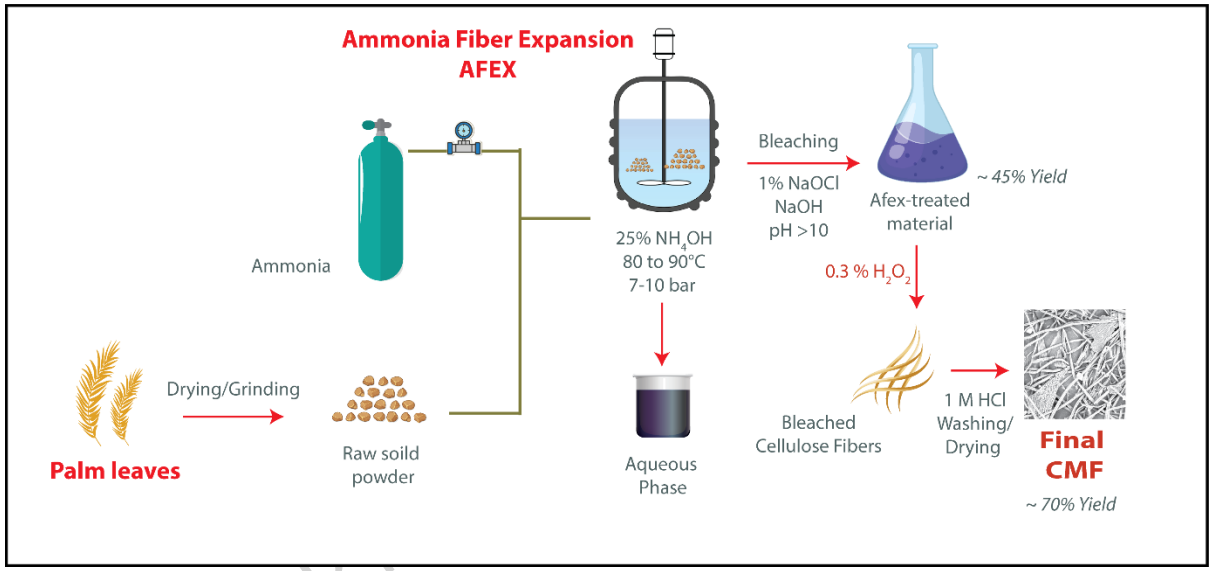

Fig. 1: Schematic representation of the experimental procedure to prepare cellulose microfibers (CMF) out of raw palm leaves using AFEX technology.

Cellulose Extraction

The AFEX-treated palm leaves were sieved and finely milled into a uniform size range of 1 to 5 mm. The bleaching process was done by mixing ~ 50 g (collected from several runs) of the treated sample with 1.2 L of 1% NaOCl (wt%), 1.0 g of NaOH, and 200 mL of distilled water, as illustrated in Fig. 1. The pH was adjusted to 10–11 to optimize the bleaching efficiency [38]. The mixture was then stirred using a mechanical stirrer at 25 °C for 48 h, as previously reported [38]. The solid white cellulose obtained from the bleaching solution was filtered and thoroughly rinsed with distilled water until a neutral solution (pH ~7) was achieved.

The filtered product was treated with 10 mL of 0.3% H_2O_2 for 1 h at room temperature (□23 ºC). H_2O_2 acts as an oxidizing agent that removes lignin and colored impurities under alkaline conditions, producing bright and pure CMF. H_2O_2 also acts as a stabilizer, preventing premature peroxide decomposition by chelating metal ions and maintaining controlled

oxidation, while a wetting agent enhances fiber penetration by increasing surface wettability and separation [17].

A second filtration was applied to extract the treated cellulose from the H_2O_2 solution. The cellulose was thoroughly rinsed with distilled water to ensure all residual chemicals were removed. The purified cellulose was then dried at 80 °C until it reached a constant weight. After drying, the cellulose was allowed to cool to room temperature and subsequently transferred to a desiccator.

After bleaching, the obtained CMF underwent acidic hydrolysis by mixing 2.5 g of bleached leaves with 500 mL of 1 M HCl and agitating the mixture at 25 °C for 2 h. The CMF was then washed 3 to 5 times with distilled water to remove residual acid and dried at 60 °C until a constant weight was achieved [38]. The percent yield for this step was ~70%.

All by-products, wastewater, and chemicals were handled and disposed of according to local regulations and standard laboratory safety procedures.

Isoconversional Analysis

Isoconversional methods, often referred to as model-free methods, are kinetic analysis approaches that determine the apparent activation energy (E_α) as a function of the conversion degree (α) without assuming any specific reaction model [26, 27]. Such methods are useful for analyzing complex or multi-step reactions, as in the case of palm leaves decomposition. Isoconversional methods can reveal how the activation energy changes with conversion and thus provide insight into possible mechanism shifts. These methods are based on the principle that, at a constant α, the reaction rate depends only on the temperature and not on the heating rate or reaction pathway temperature [26-30]. By conducting experiments at several heating rates (typically 3–5) under otherwise identical conditions, E_α values can be estimated as a function of α, enabling a more accurate description of the overall reaction kinetics [26, 27].

In this context, the degree of conversion (α) is defined as:

$$\alpha = \frac{m_0 - m}{m_0 - m_f} = \frac{\Delta m}{\Delta m_{tot}} \qquad (1)$$

where m_0 is the initial sample mass, m_f is the final mass, and m is the mass at a given time. In eqn. (1), Vyazovkin and coworkers have developed a technique to determine E_α as a function of conversion (α) based on a nonlinear (NLN) numerical integration of the rate equation of the Arrhenius form ($k_r = Ae^{-Ea/RT}$), without assuming a reaction model. Specifically, the method solves for the following equation [39, 40].

$$g(\alpha) = \frac{A_\alpha E_\alpha}{R} \sum_{j=1}^{N} J[E_\alpha, T_i(t_j)] \qquad (2)$$

where $g(\alpha)$ is the integral form of the reaction model, A_α is the conversion-dependent pre-exponential factor, $T_i(t_j)$ represents the set of temperatures at which a specific conversion fraction is reached during the i^{th} experiment, and R is the universal ideal gas constant.

The main assumption in Vyazovkin's NLN method is that the reaction model $g(\alpha)$ which is independent of the heating rate [26, 39]. Consequently, for a set of *i* experiments performed at different heating rates, $T_i(t_j)$, E_α can be determined at any specific α by identifying the value that minimizes the following function

$$\Phi(E_\alpha) = \sum_{i=1}^{n} \sum_{j\neq 1}^{n} \frac{J[E_\alpha, T_i(t_\alpha)]}{J[E_\alpha, T_j(t_\alpha)]} \qquad (3)$$

where $J[E_\alpha, T_i(t_\alpha)]$ stands for the integral $\int_{t_\alpha - \Delta_\alpha}^{t_\alpha} \exp\left(-\frac{E_\alpha}{RT_i(t)}\right)dt$. In this study, the integral was evaluated numerically based on experimental heating data divided into small time steps using Mathematica [41]. More details on the use of the NLN method can be found elsewhere [39, 40].

Another widely used integral method is the one developed by Kissinger-Akahira-Sunose (KAS), which is based on the following equation [42, 43]:

$$\ln\left(\frac{\beta_i}{T_{\alpha,i}^2}\right) = \ln\left(-\frac{A_\alpha R}{E_\alpha}\right) - \ln g(\alpha) - \left(\frac{E_\alpha}{RT_{\alpha,i}}\right) \qquad (4)$$

Here, $g(\alpha)$ is the same as defined earlier. β_i represents the heating rate, defined as $\beta_i = dT/dt$ for linear non-isothermal reactions [26, 27, 30]. The index (i) corresponds to various temperature programs, T_i is the temperature at which the (α) is achieved under the corresponding heating rate. The E_α can then be estimated from the plot of the left side of eq. (4) against $1/T_{\alpha,i}$ at a given α. These E_α values are subsequently plotted against the α values to represent the isoconversional analysis. All graphs, mathematical fittings, and integrations were done using Origin® [44].

Differential Scanning Calorimetry (DSC) Analysis

DSC is a critical thermal analysis technique used to measure heat flow changes as materials undergo transformations at varying temperatures. It provides both qualitative and quantitative data on processes such as melting, crystallization, and phase transitions [32, 45].

When there are no physical or chemical changes at a particular temperature T, the heat absorbed or released by the sample can be expressed by the equation [46]:

$$q_p = C_p \Delta T \qquad (5)$$

where q_p represents the heat flow, C_p is the specific heat capacity at constant pressure, and $\Delta T = T - T_0$ denotes the temperature change. This relationship is useful as it allows for the estimation of the amount of heat released or absorbed during a given event in the reaction. This can be determined from the area under the curve when plotting q_p (heat flow) against temperature, provided the reaction takes place at constant pressure.

Assuming that C_p remains constant within the relevant temperature range, the relationship between temperature and time can be represented as follows [46]:

$$T = T_0 + \delta t \quad (6)$$

where δ represents the scan rate. Substituting this into eqn. 6 gives

$$\Delta T = \delta t \quad (7)$$

Thermal transitions cause significant changes in the heat flow signal. During endothermic processes, such as melting, sublimation, or decomposition, the sample absorbs heat, leading to a decrease in the heat flow. In contrast, exothermic processes like oxidation, crystallization, and solid-solid transitions release heat. Depending on the instrument settings, either an upward or downward peak is observed in each case [32, 45].

Finally, the slope of the baseline line before a transition peak is indicative of the heat capacity of the substance [46]:

$$\frac{dq}{dT} = C_p \quad (8)$$

This relationship is important for determining the thermal stability and heat capacity of materials, including the palm leaves samples. The enthalpy change related to thermal transitions quantifies the energy required for a phase change to occur. Understanding this energy measurement is essential for evaluating the material's stability under varying thermal conditions.

3. Results and Discussion

3.1 Material Characterizations

The SEM images presented in Fig. 2 show the structural differences between the raw palm leaves and the synthesized CMF at the microscopic level. The raw material (a and b) exhibits the typical structure of plant fibers with a rough and irregular surface, containing numerous pores. The produced CMF (c and d) appear as elongated, uniformly shaped fibers with smooth surfaces. It is also interesting to observe that many of these fibers are bundled into larger strands. The length of individual fibers ranged from 0.1 to 3.0 mm, with diameters between 5 and 20 µm. The diameter of the obtained CMF is close to what was obtained by Giri et al. (~5 µm) [45], and Abzan *et al*. (10-15 µm) [47]. However, the fibers produced in this study exhibited substantially greater lengths (0.03–0.3 mm for Giri *et al*. [45]. The size of the obtained CMF suggests that these fibers have potential for use in future applications, particularly in the paper and pharmaceutical industries [12-14]. Further comparison between the raw palm leaves and the produced CMF in this study is shown in Table 1.

Table 1: *A side-by-side comparison of raw palm leaves versus the obtained CMF.*

Property		**Raw Palm leaves**	**CMF**
C/O ratio		1.8 ± 0.2	2.8 ± 0.3
Microstructure		Irregular fibers	Elongated fibers
FTIR Bands (cm^{-1})			

	3300–3500	O-H (hydroxyl/water)	Reduced
	2918, 2850	C-H (alkanes/carboxylic acids)	Decreased
	1633, 1600–1700	C=O (lignin)	Removed
	1000–1200	C-O (cellulose/hemicellulose)	Weaker
	1000–1600	Minor	Reduced
DSC area (a.u)		Lower energy content (3107)	Higher energy content (3411)
Activation energies (E_α) kJ mol^{-1}		Higher	Lower

 At 25 °C min^{-1}

The EDX analysis shown in Fig. S1-S6 in the *supplementary materials* shows differences between raw and treated palm leaves. In particular, it was observed that the carbon/oxygen ratio (C/O) changed notably after the treatment. Palm leaves are mainly composed of lignin (32.5%), hemicellulose (23%), and cellulose (44.5%) [48, 49]. The C/O ratios in cellulose, lignin, and hemicellulose are 0.75, 2.1, and 0.95, respectively. According to EDX analysis, the raw material had an average C/O ratio of 1.8±0.2, which increased to 2.8 ± 0.3 after the AFEX/bleaching treatment. The carbon ratio in the synthesized CMF exceeds that of any of the three components.

This increase likely reflects real chemical restructuring rather than an analytical artefact. The combined AFEX and acid hydrolysis treatment can promote dehydration, decarboxylation, and condensation reactions, consistent with known acid-catalyzed sugar degradation mechanisms. AFEX pretreatment increases accessibility and reduces crystallinity, facilitating these reactions during subsequent acid hydrolysis. Notably, SEM-EDX probes a subsurface region (typically 0.3 µm to a few micrometers), providing insight into near-surface composition rather than just the outermost layer.

The elevated carbon content in the synthesized CMF suggests enhanced thermal stability, conductivity, and heat capacity process [11, 48, 50, 51], as discussed in the following sections.

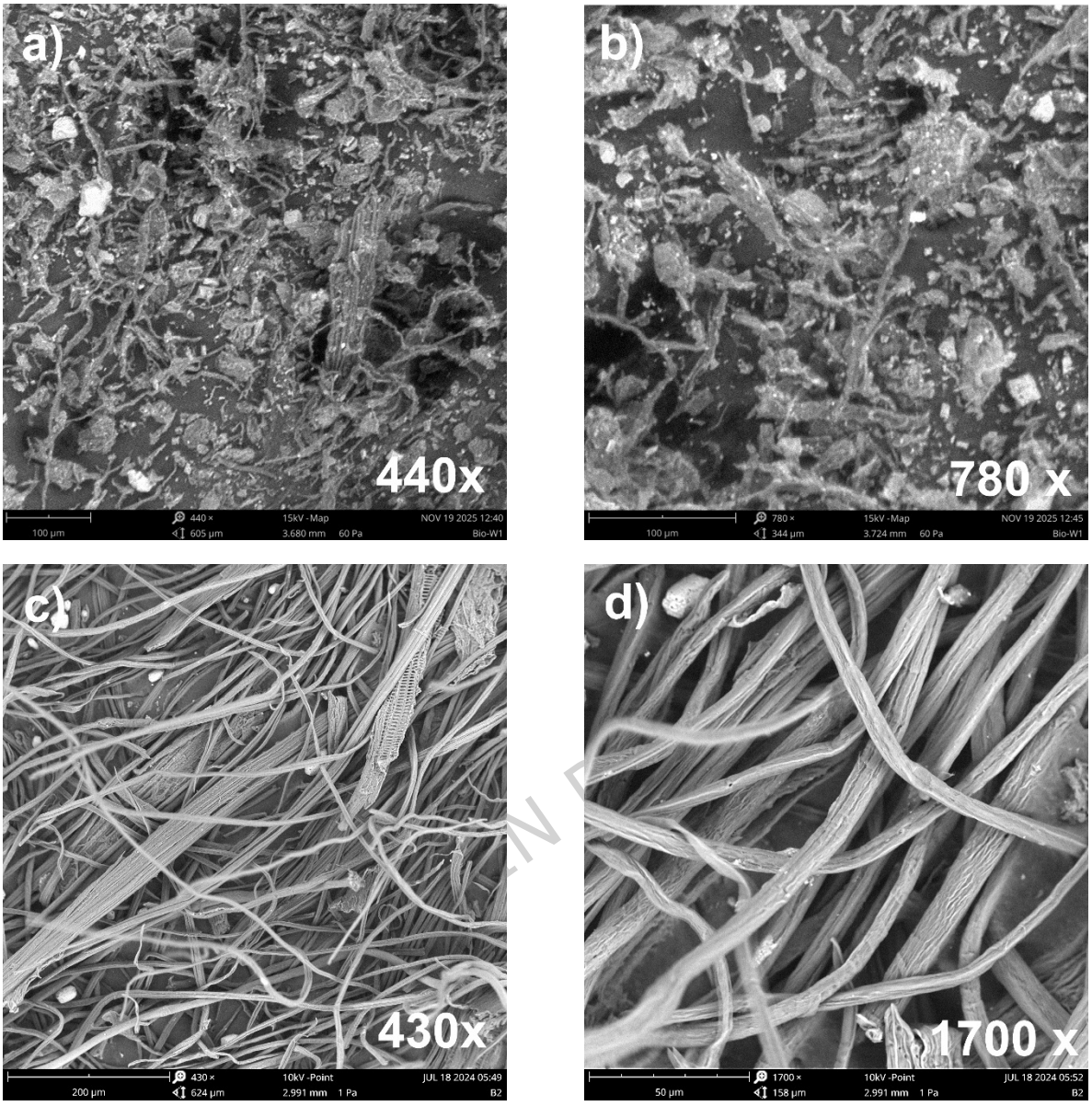

Fig. 2: SEM images at different magnifications of a-b) raw palm leaves, and c-d) cellulose microfibers (CMF). EDX measurements are provided in the Supplementary Materials.

The above findings are consistent with our observations from the FTIR analysis. Fig. S2 provides further insights into the chemical changes induced by the treatment of raw palm leaves. The FTIR spectrum of the raw palm leaves (Fig. S2-a) shows a broad O-H stretching band (~3300-3500 cm^{-1}), indicative of water content and/or hydrogen-bonded hydroxyl groups, which are characteristic of the hydroxyl-rich structure of cellulose and hemicellulose [18]. Additionally, two prominent bands at 2918 and 2850 cm^{-1} are observed, corresponding to C-H stretching vibrations in alkanes, aldehydes, or carboxylic acids [18]. The presence of carboxylic acids is further supported by a band at 1633 cm^{-1}, which falls within the 1600-1700 cm^{-1} region typically associated with carbonyl (C=O) groups. This band strongly suggests that the raw material is rich in lignin, as lignin is known to contain abundant conjugated carbonyls [18, 48, 49, 51].

The FTIR spectrum of the AFEX-treated material (before bleaching) is shown in Fig. S2-b. The signal intensity is notably enhanced compared to that of the raw material, with pronounced bands in the 1000-1600 cm^{-1} region. These changes reflect the chemical modifications to the plant structure resulting from ammonia treatment under high pressure. The bands in this region are indicative of the formation of various nitro, carbonyl, and aromatic functional groups. Specifically, bands in the 1000-1200 cm^{-1} range correspond to C-O stretching vibrations, which are characteristic of the polysaccharide backbone of cellulose and hemicellulose, confirming the presence of glycosidic linkages. This is in agreement with the CMF characterization reported by Bahloul *et al.* and Sajid *et al.* [17, 52].

Finally, Fig. S2-c shows the FTIR spectrum of the CMF produced after bleaching the AFEX-treated samples. The intensity of most bands has either diminished or disappeared entirely, particularly those in the 1600-1700 cm^{-1} and 2800 cm^{-1} regions. This observation suggests the effective removal of lignin and hemicellulose during the bleaching process. These results are in excellent agreement with our conclusion that bleaching effectively removes oxygenated functional groups, thereby enriching the carbon percentage in the sample. This finding highlights the efficiency of the treatment process in significantly increasing the carbon content of the final product.

3.3 DSC Analysis and Heat Content Assessment

The DSC thermograms for the raw material and the synthesized CMF are depicted in Fig. 3. The data were fitted at two heating rates of 10 and 25 °C min^{-1} to ensure a fair comparison. The thermograms show distinct endothermic peaks at around 350 and 400°C. The first peak agrees well with the reported thermal degradation temperatures (T_d) of the CMF [18, 53]. As previously described in the DSC analysis (Section 3.5), it is possible to estimate the amount of heat in DSC curves by calculating the area under the curve of q_p against temperature. Using Origin ® software package [44], the integrated area under the curves and the corresponding numbers are shown in Fig. 3 in arbitrary units. The CMF exhibits a higher heat content than the raw material under identical conditions. The DSC analysis was conducted at three different heating rates, and the previous observation remained consistent. This can be attributed to the higher carbon content in the *bleached* CMF, which contributes to its greater heat value compared to the raw material [11, 51]. This increase in heat content makes the CMF a potentially valuable material for energy-related applications, such as biofuels or energy storage, where a higher calorific value is desirable.

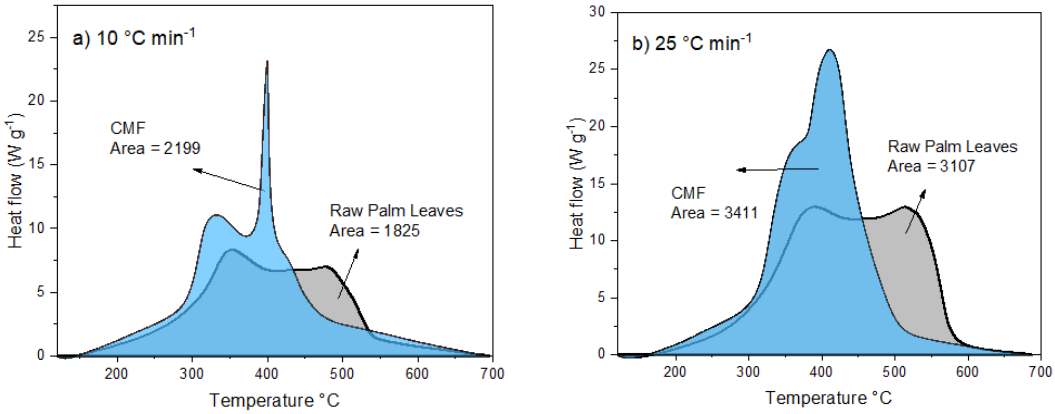

Fig. 3: DSC curves for raw and bleached palm leaves at a) 10 °C min^{-1}, b) 15 °C min^{-1}, c) 20 °C min^{-1}, and d) 25 °C min^{-1}.

3.2 Isoconversional Kinetics

Fig. 4 illustrates the TGA thermograms for the raw palm leaves (a) and the synthesized CMF (b), under air flow of 100 mL min^{-1}, in the temperature range of 180-720 °C and at different heating rates of 5, 10, and 25 °C min^{-1}. As seen, the sample temperature increases at the set heating rate. This behavior suggests that the decomposition of palm leaves is kinetically controlled, as the process depends not only on temperature but also on reaction time, which is influenced by the heating rate. The derivative thermogravimetry (DTG) curve (blue) for raw palm leaves exhibits three distinct peaks at approximately 260, 410, and 630 °C, whereas for CMF, four peaks appear at higher temperatures of 360, 460, 530, and 680 °C. These observations reflect the structural and chemical modifications that the material has undergone during thermo-oxidative decomposition.

Upon comparing the thermograms of raw palm leaves and CMF, it is evident that CMF begins to decompose at a slightly higher temperature. This difference, along with the distinct decomposition profile, is attributed to variations in composition and thermal reactivity between the two materials. The higher onset temperatures (T_{onset}) observed for CMF suggest enhanced thermal stability, which can be attributed to the increased carbon content, as mentioned earlier. This finding is also in agreement with our subsequent DSC analysis.

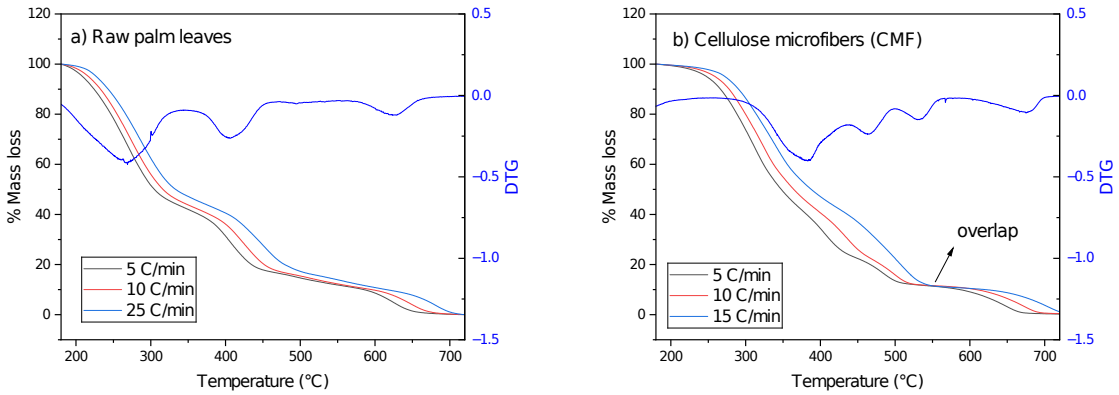

Fig. 4: TGA curves for a) raw palm leaves and b) cellulose microfibers (CMF), under air flow of 100 mL min^{-1}, at different heating rates of 10, 15, 20, and 25 °C min^{-1}.

The isoconversional analysis of the TGA data was performed as outlined in the previous section. As reported, applying the isoconversional method requires using 3–5 heating rates, where the curves should be well-separated [26, 27]. Fig. 5 shows the extent of conversion (α) as a function of temperature at different heating rates for both the raw palm leaves and CMF. The curves demonstrate clear separation within almost the entire α range between 0.05 and 0.9. However, the curves for CMF demonstrate areas of overlap around 0.9 due to the complex reactions taking place in the region. Therefore, the isoconversional analysis was done for the full range between 0.05 and 0.9 for the raw material, and over the same range for CMF, except for α between 0.85 and 0.95.

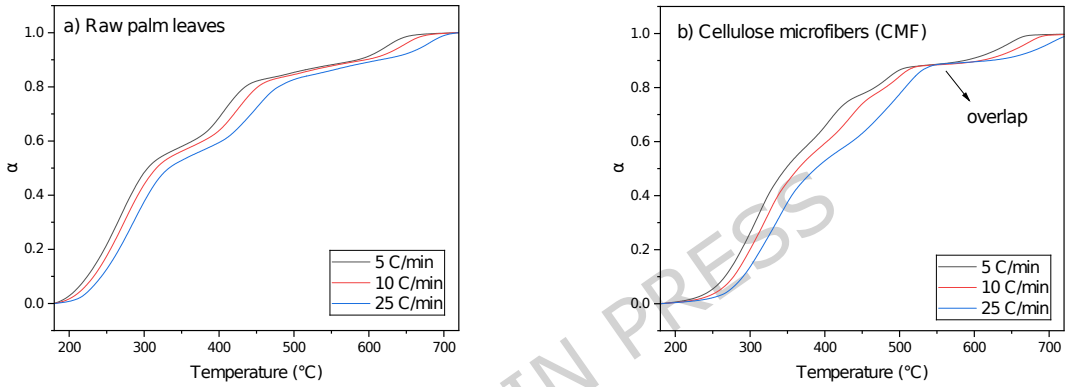

Fig. 5: The conversion degree (α) as a function of temperature at varying heating rates in the presence of air flow of 100 mL min^{-1} for: a) raw palm leaves and b) cellulose microfibers (CMF).

Following the KAS method, plotting ln □ against 1/T at each value of α, E_α is obtained from the slope of the best-fit line for both raw material and CMF as shown in Fig S8 (supplementary information section). All linear fittings were acceptable with $R^2 > 0.99$ (for KAS), and were numerically optimized to a minimum using nonlinear regression for NLN.

Fig. 5, shows the E_α values obtained by the NLN and KAS methods for both the raw palm leaves and CMF as a function of α. As seen, the E_α values obtained by the KAS method were identical to those obtained by the NLN method. This observation comes as no surprise, as the KAS method was developed to solve the same fundamental kinetic equations as the NLN approach, although using a different mathematical approximation (linearization against non-linear optimization) [40, 54, 55]. Furthermore, the KAS method produced nearly identical E_α values to NLN, particularly at low-to-moderate conversions, where the linear approximation in KAS remains valid [39, 55]. However, minor deviations, as in our case (*cf.* Fig. 5), may arise at higher α due to the NLN method's superior handling of variable activation energies in multi-step processes.

It is noteworthy that the E_α values obtained in this study for CMF (100–150 kJ·mol^{-1}) were lower than those reported by Barud *et al.* for commercial microcrystalline cellulose, which ranged from 175 to 185

kJ·mol^{-1} [56]. Barud *et al*. employed the Capela-Ribeiro isoconversional method in their study.

The trend shown in Fig. 6 indicates that the E_α values vary throughout the reaction, indicating a switch in the reaction pathways. This variation reflects the presence of complex reaction mechanisms [29, 30, 57]. Also, the figure shows that the E_α values for the reaction of CMF are lower than those obtained for the raw palm leaves, particularly during the initial and middle stages of the reaction (up to α≈0.7, T≈450 °C). Under such conditions, the thermal degradation of organic compounds dominates over oxidation, as the latter requires higher temperatures [30, 58, 59].

As shown in Fig. 6 the E_α values exhibit a sharp increase at higher conversion levels (α>0.75), corresponding to temperatures above 450 °C. This spike coincides with the second DTG peak observed for both the raw palm leaves and CMF (see Fig. 2). Notably, the CMF displays multiple DTG peaks at elevated temperatures, along with a distinct overlapping degradation region around 550 °C. These observations suggest that the material undergoes a complex oxidation process at this stage, likely involving the oxidation of more stable intermediate products formed during the primary degradation phase at lower temperatures.

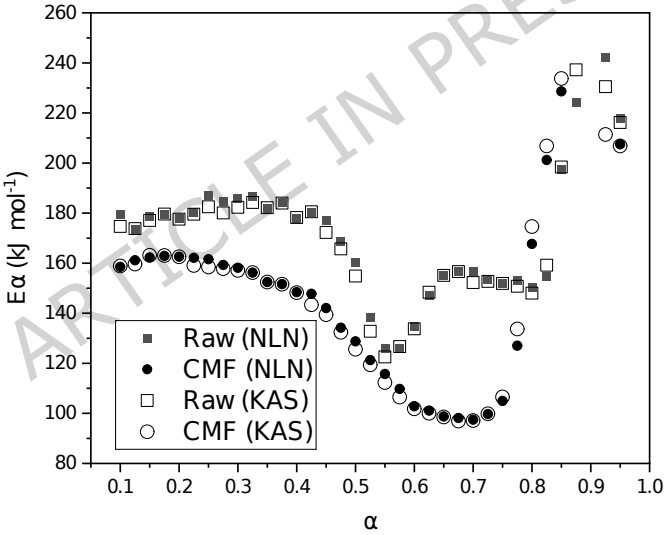

Fig. 6: The effective activation energy profiles (E_α) for the oxidative decomposition of palm leaves and CMF under air flow between 120 and 690 °C using a) the NLN and b) KAS methods. Standard deviations of E_α values were in the range of 1-4 kJ mol^{-1}. Error bars are not shown for clarity purposes

3.3 Kinetic modeling and determination of the kinetic triplet

The isoconversional method serves as a tool to identify the reaction model and determine kinetic parameters, including A_α, $\Delta H^{\neq}$, $\Delta S^{\neq}$, and $\Delta G^{\neq}$[28, 29, 35, 57]. The entropy of activation ($\Delta S^{\neq}$) is related to the unimolecular pre-exponential factor A_{uni} by [46]:

$$A_{uni} = \left(\frac{e k_B T}{h}\right) e^{\Delta S^{\neq}/R} \qquad [9]$$

here, e is Euler's number (2.7183), k_B is Boltzmann's constant, h is Planck's constant, and R is the ideal gas constant. Rearranging eqn. 9 allows for calculating the entropy of activation $\Delta S^{\neq}$ [46]:

$$\Delta S^{\neq} = R\left(\ln\frac{Ah}{ek_BT}\right) \quad [10]$$

The y-intercept of the best-fit-line firing of eq. 4 corresponds to $\ln\left(-\frac{A_\alpha R}{E_\alpha}\right)$.

Therefore, A_α (A_{uni}) and $\Delta S^{\neq}$ were calculated.

Additionally, the enthalpy $\Delta H^{\neq}$ and Gibbs free energy $\Delta G^{\neq}$ of activation can be derived using the following equations [46]:

$$E_{\square} = \Delta H^{\neq} + RT \quad [11]$$

$$\Delta G^{\neq} = \Delta H^{\neq} - T\Delta S^{\neq} \quad [12]$$

The calculated kinetic parameters are all tabulated in Table 2.

Table 2: *Kinetic parameters were determined by combining the KAS equation with model fitting at α=0.5, for raw and CMF.*

Samples	**Raw**	**CMF**
T (°C)	346.7	346.7
A_α (s^{-1})	2.8×10^{13}	7.4×10^{9}
$\Delta S^{\neq}$ (J mol^{-1} K^{-1})	-237.7	-240.3
$\Delta H^{\neq}$ (kJ mol^{-1})	149.7	120.4
$\Delta G^{\neq}$ (kJ mol^{-1})	297.0	269.4

The kinetic study reveals notable differences between the raw material and CMF under oxidative conditions, as shown in Table 2. At 50% conversion, raw palm leaves exhibit a considerably larger pre-exponential factor (A_α) of 2.8×10^{13} s^{-1}, compared to 7.4×10^{9} s^{-1} for CMF. This difference can be attributed to the bleaching procedure, which alters the molecular structure and reaction pathways, leading to a significant reduction in A_α for the bleached sample. Additionally, the activation entropy ($\Delta S^{\neq}$) values for the raw palm leaves and CMF samples are similar, measured at -237.7 and -240.3 J mol^{-1} K^{-1}, respectively. The negative $\Delta S^{\neq}$ values indicate that the activated complexes possess lower entropy (i.e., higher molecular order) compared to the reactants.

Table 2 also presents a comprehensive comparison of the thermodynamic parameters $\Delta H^{\neq}$ and $\Delta G^{\neq}$ for raw and bleached palm leaves under oxidative conditions. Raw palm leaves exhibit a significantly higher enthalpy of activation ($\Delta H^{\neq}$) of 149.7±3.9 kJ mol^{-1}, compared to 120.4 ±3.9 kJ mol^{-1} for the bleached samples. This difference is related to the dependence of $\Delta H^{\neq}$ on the activation energy (E_α), as described by eq. 12. The higher $\Delta H^{\neq}$ for raw palm leaves indicates that more energy is required to reach the transition state, likely due to the structural complexity and stronger molecular interactions inherent in the untreated biomass. On the

other hand, the bleached palm leaves, with their simplified structure, require less energy for decomposition, as reflected in the lower $\Delta H^{\neq}$ value.

Using eq. 12, the Gibbs free energy of activation ($\Delta G^{\neq}$) was calculated. The $\Delta G^{\neq}$ value for raw palm leaves was 297.0±3.9 kJ mol^{-1}, while the CMF sample exhibited a slightly lower value of 269.4 kJ/mol. According to eq. 12, $\Delta G^{\neq}$ depends on both the enthalpy of activation ($\Delta H^{\neq}$) and the activation entropy ($\Delta S^{\neq}$). Since the $\Delta S^{\neq}$ values for both samples were similar, the observed difference in $\Delta G^{\neq}$ can be mainly attributed to variations in $\Delta H^{\neq}$.

The value of $\Delta H^{\neq}$ (149.7±3.9 kJ mol^{-1}) for the raw material is higher than that for CMF ($\Delta H^{\neq}$ = 120.4±3.9 kJ mol^{-1}). This suggests that more energy is required to break down the palm leaves lignocellulosic matrix, which is more resistant to thermal degradation. In contrast, CMF decomposes more readily, requiring less energy input for the same process.

Table 3 shows a comparison of the CMF obtained in this study with those reported in the literature from different tree leaves. The CMF produced in this study showed high thermal stability, good yield (70%), and relatively low activation energy of decomposition (100–150 kJ·mol^{-1}) compared to other sources. These characteristics indicate that the CMFs have good potential for industrial and biochemical applications. With that being said, future work is needed to scale up the process the industrial level. This includes handling ammonia at high pressure, the associated safety requirements, and the capital cost of installing efficient ammonia-recovery systems. We also note, however, that AFEX remains one of the few pre-treatment techniques where over 95% of the ammonia can be recovered. which substantially mitigates both cost and safety concerns at scale [20, 21]. Modern AFEX units already operate with established engineering controls, making the process manageable and comparable in safety to other high-pressure processes.

Table 3: *Comparison of CMFs from tree leaves and those obtained from the literature*

Name of tree leaves	CMF diameter (µm)	CMF length (µm)	Method	Yield (%)	Crystallinity%	
Palm leaf (*Phoenix dactylifera L.*) were	5-20	0.1-0.3	AFEX/Bleaching	70%	75%	
Banana Plant Leaves (Musa balbisiana Colla)	2-8	-	Alkaline hydrolysis + Bleaching	-	65%	[
Washingtonia Palm (Petiole fibers)	6 - 20.5		Alkaline hydrolysis + Bleaching	39	65%	[
Cherry Plum (*Prunus cerasifera pissardi nigra*),	0.3-0.6	-	Alkaline hydrolysis + Bleaching	19-26%	-	[

White Mulberry (*Morus alba*), Plane (*Platanus orientalis*)						
doum tree (Chamaerops humilis var. argentea	3-10	0.45	Alkaline hydrolysis + Bleaching	-	76-80%	[
Wheat Stalk	4.7-5.0	25 ± 5	Alkaline hydrolysis + Bleaching	-	Crystalline	[
Gluconacetobacter xylinus bacteria	-	-	Commercial	-	78%	[
Shrub (*Cistus ladanifer L. and Erica arborea L.*)	9,20 - 15,30	100 - 110	Alkaline hydrolysis + Bleaching	51,5%	72.4-81.0 %	[

Conclusion

The study presented a new pathway to fabricate high-quality cellulose microfibers (CMF). The nanofibers were produced by first treating raw palm leaves with AFEX, followed by bleaching and acid hydrolysis. The novelty of this work lies in the specific application of the AFEX pretreatment to palm leaves, a highly abundant but underutilized agricultural residue, which effectively disrupts the lignocellulosic structure and facilitates the subsequent efficient extraction of CMF.

SEM characterization of the final CMF showed a transition from the irregular and porous architecture characteristic of raw palm leaves to the formation of elongated, uniformly contoured CMF (with dimensions 0.1–3.0 mm in length, and 5–20 µm diameter), often naturally aggregating into bundles, and exhibiting notably smooth surface topographies.

Further EDX and FTIR analysis confirmed the elimination of lignin and hemicellulose during the treatment, indicating an increase in the carbon content in the CMF. This carbon enrichment strengthens the material and increases its heat value. This chemical purification directly translated to enhanced material properties: the CMF demonstrated higher thermal stability and a greater heat content than the raw biomass, as revealed by TGA and DSC analyses.

The kinetic analysis provided critical insights for future scale-up. The use of advanced isoconversional methods (Vyazovkin NLN and KAS) revealed a complex, multi-step decomposition mechanism for both raw and treated materials. It was found that the effective activation energy values (E_α) of the thermal decomposition of both the raw leaves and the CMF change as the reaction progresses, indicating a multi-step mechanism. Furthermore, the E_α values for CMF (100–150 kJ·mol^{-1}) were lower than those of the raw material. The high stability, low activation energies, along with our high yield of 70% and the fact that the reaction follows a very orderly path, give us a solid practical foundation to scale this process up for industrial use.

The kinetic modeling also involved the determination of the kinetic parameters A_α, $\Delta S^{\#}$, $\Delta H^{\#}$, and $\Delta G^{\#}$. The entropy of activation ($\Delta S^{\#}$) values were negative for both CMF and raw material, indicating the formation of a more ordered activated complex. The enthalpy of activation ($\Delta H^{\#}$) of the raw leaves was higher than that for CMF, in agreement with the experimental E_α values. Because $\Delta S^{\#}$ for the raw material and CMF were close, the $\Delta G^{\#}$ was enthalpy dependent.

The features of the synthesized CMF make it promising for different industrial applications, such as the pulp and paper and pharmaceutical industries and the energy sector. In addition, the kinetic insights gained provide a foundation for scaling up palm leaves conversion into CMF.

Acknowledgements

The authors are grateful to the Department of Chemistry and the Faculty of Science at An-Najah National University, the Department of Chemical and Petroleum Engineering, University of Calgary, and the Natural Sciences and Engineering Research Council of Canada (NSERC) for their support of this project. Further thanks are due to Prof. Nidal Jaradat, Mr. Ahmed Mehairi, Mr. Tamer Al-Shboul, and Mr. Ameed Amireh for his valuable assistance in this work.

Ethics approval and consent to participate.

The palm leaves samples were collected with the permission of the landowner, Dr. Derar Al-Smadi, from his property located in Jiftlik, Jericho, Palestine.

Consent for publication

Not applicable

Availability of data and materials

All data generated or analyzed during this study are included in this published article [and its supplementary information files].

Competing interests

The authors declare that they have no competing interests.

Funding

Non available

Authors' contributions

IB: conceptualization, resources, supervision, writing, DY, AM, DS, KH, formal analysis, visualization, validation, writing, NN, conceptualization, project administration, resources, validation, writing.

Conflicts of interest

The authors declare that there is no conflict of interest regarding the publication of this article.

References

1. Springmann M, Clark M, Mason-D'Croz D, Wiebe K, Bodirsky BL, Lassaletta L, de Vries W, Vermeulen SJ, Herrero M, Carlson KM *et al*: **Options for keeping the food system within environmental limits**. *Nature* 2018, **562**(7728):519-525.
2. Vermeulen SJ, Campbell BM, Ingram JSI: **Climate Change and Food Systems**. *Annual Review of Environment and Resources* 2012, **37**(Volume 37, 2012):195-222.
3. Foley JA, DeFries R, Asner GP, Barford C, Bonan G, Carpenter SR, Chapin FS, Coe MT, Daily GC, Gibbs HK *et al*: **Global Consequences of Land Use**. *Science* 2005, **309**(5734):570-574.
4. Abubakar IR, Maniruzzaman KM, Dano UL, AlShihri FS, AlShammari MS, Ahmed SMS, Al-Gehlani WAG, Alrawaf TI: **Environmental Sustainability Impacts of Solid Waste Management Practices in the Global South**. *International Journal of Environmental Research and Public Health* 2022, **19**(19):12717.
5. Sharma B, Vaish B, Monika, Singh UK, Singh P, Singh RP: **Recycling of Organic Wastes in Agriculture: An Environmental Perspective**. *International Journal of Environmental Research* 2019, **13**(2):409-429.
6. Wiedinmyer C, Yokelson RJ, Gullett BK: **Global Emissions of Trace Gases, Particulate Matter, and Hazardous Air Pollutants from Open Burning of Domestic Waste**. *Environ Sci Technol* 2014, **48**(16):9523-9530.
7. Nugraha MG, Mozasurya ED, Hidayat M, Saptoadi H: **Evaluation of combustion characteristics in biomass residues open burning**. *Materials Today: Proceedings* 2023, **87**:45-50.
8. Food Agriculture Organization of the United Nations: **World Food and Agriculture-Statistical Yearbook 2024**. Rome, Italy: Food and Agriculture Organization of the United Nations (FAO).
9. Jonoobi M, Shafie M, Shirmohammadli Y, Ashori A, Hosseinabadi HZ, Mekonnen T: **A review on date palm tree: Properties, characterization and its potential applications**. *Journal of Renewable Materials* 2019, **7**(11):1055-1075.
10. Jeguirim M, Khiari B, Jellali S: **Chapter 1 - Identification, Quantification and Characterization of palm-tree and fruit wastes**. In: *Palm Trees and Fruits Residues.* Edited by Jeguirim M, Khiari B, Jellali S: Academic Press; 2023: 1-58.
11. Klemm D, Kramer F, Moritz S, Lindström T, Ankerfors M, Gray D, Dorris A: **Nanocelluloses: A New Family of Nature-Based Materials**. *Angew Chem Int Ed* 2011, **50**(24):5438-5466.
12. Ling S, Kaplan DL, Buehler MJ: **Nanofibrils in nature and materials engineering**. *Nature Reviews Materials* 2018, **3**(4):18016.
13. Heise K, Kontturi E, Allahverdiyeva Y, Tammelin T, Linder MB, Nonappa, Ikkala O: **Nanocellulose: Recent Fundamental**

Advances and Emerging Biological and Biomimicking Applications. *Adv Mater* 2021, **33**(3):2004349.

14. Thomas P, Duolikun T, Rumjit NP, Moosavi S, Lai CW, Bin Johan MR, Fen LB: **Comprehensive review on nanocellulose: Recent developments, challenges and future prospects**. *Journal of the Mechanical Behavior of Biomedical Materials* 2020, **110**:103884.
15. Siouri F, Abujaber F, Jaradat M, Mubarak A: **Eco-Friendly and Efficient Extraction of Parabens from Cream Products Using Magnetic Cellulose Nanoparticles: A Promising Analytical Method**. *An-Najah University Journal for Research - A (Natural Sciences)* 2025, **40**(1).
16. Pawaskar P, Lekurwale S, Kumari M, Roy S, Banerjee S: **Isolation of cellulose microfibers from banana plant residues and their conversion into sustainable and biocompatible 3D printable hydrogels for drug delivery**. *Industrial Crops and Products* 2025, **229**:120998.
17. Sajid L, Azmami O, Ahmadi ZE, Benayada A, Boukhriss A, Majid S, Gmouh S: **Extraction and application of cellulose microfibers from Washingtonia palm as a reinforcement of starch film**. *Journal of Plastic Film & Sheeting* 2021, **37**(4):529-558.
18. Celik S, Kutlu G, Tornuk F: **Recovery and characterization of cellulose microfibers from fallen leaves and evaluation of their potential as reinforcement agents for production of new biodegradable packaging materials**. *Food Science & Nutrition* 2024, **12**(10):8364-8376.
19. Wang Z, Tammela P, Strømme M, Nyholm L: **Cellulose-based Supercapacitors: Material and Performance Considerations**. *Advanced Energy Materials* 2017, **7**(18):1700130.
20. Wang G, Dai Y, Yang H, Xiong Q, Wang K, Zhou J, Li Y, Wang S: **A Review of Recent Advances in Biomass Pyrolysis**. *Energy & Fuels* 2020, **34**(12):15557-15578.
21. Mokomele T, da Costa Sousa L, Bals B, Balan V, Goosen N, Dale BE, Görgens JF: **Using steam explosion or AFEX™ to produce animal feeds and biofuel feedstocks in a biorefinery based on sugarcane residues**. *Biofuels, Bioproducts and Biorefining* 2018, **12**(6):978-996.
22. Balan V, Bals B, Chundawat SPS, Marshall D, Dale BE: **Lignocellulosic Biomass Pretreatment Using AFEX**. In: *Biofuels: Methods and Protocols.* Edited by Mielenz JR. Totowa, NJ: Humana Press; 2009: 61-77.
23. Campbell TJ, Teymouri F, Bals B, Glassbrook J, Nielson CD, Videto J: **A packed bed Ammonia Fiber Expansion reactor system for pretreatment of agricultural residues at regional depots**. *Biofuels* 2013, **4**(1):23-34.
24. Avci U, Zhou X, Pattathil S, da Costa Sousa L, Hahn MG, Dale B, Xu Y, Balan V: **Effects of extractive ammonia pretreatment on the**

ultrastructure and glycan composition of corn stover. *Frontiers in Energy Research* 2019, **7**:85.

25. Lau MJ, Lau MW, Gunawan C, Dale BE: **Ammonia Fiber Expansion (AFEX) Pretreatment, Enzymatic Hydrolysis, and Fermentation on Empty Palm Fruit Bunch Fiber (EPFBF) for Cellulosic Ethanol Production**. *Appl Biochem Biotechnol* 2010, **162**(7):1847-1857.
26. Vyazovkin S: **Isoconversional kinetics of thermally stimulated processes**. New York, NY, USA: Springer; 2015.
27. Vyazovkin S, Burnham AK, Favergeon L, Koga N, Moukhina E, Pérez-Maqueda LA, Sbirrazzuoli N: **ICTAC Kinetics Committee recommendations for analysis of multi-step kinetics**. *Thermochim Acta* 2020, **689**:178597.
28. Badran I, Nassar NN, Marei NN, Hassan A: **Theoretical and thermogravimetric study on the thermo-oxidative decomposition of Quinolin-65 as an asphaltene model molecule**. *RSC Adv* 2016, **6**(59):54418-54430.
29. Badran I, Manasrah AD, Hassan A, Nassar NN: **Kinetic study of the thermo-oxidative decomposition of metformin by isoconversional and theoretical methods**. *Thermochim Acta* 2020, **694**:178797.
30. Riyaz NS, Badran I: **The catalytic thermo-oxidative decomposition of glimepiride using the isoconversional method**. *J Therm Anal Calorim* 2022, **147**(19):10755-10765.
31. Manasrah AD, Hassan A, Nassar NN: **Enhancement of petroleum coke thermal reactivity using Oxy-cracking technique**. *Can J Chem Eng* 2019, **97**(11):2794-2803.
32. Höhne GWH, Hemminger WF, Flammersheim HJ: **Theoretical Fundamentals of Differential Scanning Calorimeters**. In: *Differential Scanning Calorimetry.* Edited by Höhne GWH, Hemminger WF, Flammersheim HJ. Berlin, Heidelberg: Springer Berlin Heidelberg; 2003: 31-63.
33. Hawash M, Jaradat N, Salhi NA, Shatreet B, Asbah AA, Hawash YH: **Assessing the therapeutic potential and safety of traditional anti-obesity herbal blends in Palestine**. *Sci Rep* 2024, **14**(1):1919.
34. Jaradat NA, Zaid AN, Al-Ramahi R, Alqub MA, Hussein F, Hamdan Z, Mustafa M, Qneibi M, Ali I: **Ethnopharmacological survey of medicinal plants practiced by traditional healers and herbalists for treatment of some urological diseases in the West Bank/Palestine**. *BMC Complementary and Alternative Medicine* 2017, **17**(1):255.
35. Nassar NN, Hassan A, Vitale G: **Comparing kinetics and mechanism of adsorption and thermo-oxidative decomposition of Athabasca asphaltenes onto TiO2, ZrO2, and CeO2 nanoparticles**. *Applied Catalysis A: General* 2014, **484**:161-171.

36. Nassar NN, Hassan A, Pereira-Almao P: **Metal Oxide Nanoparticles for Asphaltene Adsorption and Oxidation**. *Energy & Fuels* 2011, **25**(3):1017-1023.
37. Hamed OA, Fouad Y, Hamed EM, Al-Hajj N: **Cellulose powder from olive industry solid waste**. *BioResources* 2012, **7**(3):4190-4201.
38. Hamed OA, Jodeh S, Al-Hajj N, Hamed EM, Abo-Obeid A, Fouad Y: **Cellulose acetate from biomass waste of olive industry**. *Journal of Wood Science* 2015, **61**(1):45-52.
39. Nassar NN, Hassan A, Luna G, Pereira-Almao P: **Comparative study on thermal cracking of Athabasca bitumen**. *J Therm Anal Calorim* 2013, **114**(2):465-472.
40. Vyazovkin S: **Modification of the integral isoconversional method to account for variation in the activation energy**. *J Comput Chem* 2001, **22**(2):178-183.
41. Wolfram Research I: **Mathematica**. In., vol. Version 13.1. Champaign, Illinois: Wolfram Research, Inc.; 2022.
42. Blaine RL, Kissinger HE: **Homer Kissinger and the Kissinger equation**. *Thermochim Acta* 2012, **540**:1-6.
43. Kissinger HE: **Reaction kinetics in differential thermal analysis**. *Anal Chem* 1957, **29**(11):1702-1706.
44. OriginLab: **Origin: Scientific Data Analysis and Graphing Software**. In., 2024 edn: OriginLab; 2024.
45. Gill PS, Sauerbrunn SR, Reading M: **Modulated differential scanning calorimetry**. *J Therm Anal* 1993, **40**(3):931-939.
46. Atkins PW, De Paula J, Keeler J: **Atkins' physical chemistry**. Oxford, United Kingdom ; New York, NY: Oxford University Press; 2023.
47. Abzan N, Abbasian A, Jonoobi M, Ghasemi I: **Cellulose microfiber extraction from leftover celery pulp: Chemomechanical treatments, structural, morphological, and thermal characterization**. *Int J Biol Macromol* 2023, **253**:126834.
48. Ameen M, Zamri NM, May ST, Azizan MT, Aqsha A, Sabzoi N, Sher F: **Effect of acid catalysts on hydrothermal carbonization of Malaysian oil palm residues (leaves, fronds, and shells) for hydrochar production**. *Biomass Conversion and Biorefinery* 2022, **12**(1):103-114.
49. Nizamuddin S, Jayakumar NS, Sahu JN, Ganesan P, Bhutto AW, Mubarak NM: **Hydrothermal carbonization of oil palm shell**. *Korean J Chem Eng* 2015, **32**(9):1789-1797.
50. Qureshi SS, Nizamuddin S, Baloch HA, Siddiqui MTH, Mubarak NM, Griffin GJ: **An overview of OPS from oil palm industry as feedstock for bio-oil production**. *Biomass Conversion and Biorefinery* 2019, **9**(4):827-841.
51. Zhang T, Wu X, Luo T: **Polymer Nanofibers with Outstanding Thermal Conductivity and Thermal Stability: Fundamental**

Linkage between Molecular Characteristics and Macroscopic Thermal Properties. *J Phys Chem C* 2014, **118**(36):21148-21159.

52. Bahloul A, Kassab Z, Aziz F, Hannache H, Bouhfid R, Qaiss AEK, Oumam M, El Achaby M: **Characteristics of cellulose microfibers and nanocrystals isolated from doum tree (Chamaerops humilis var. argentea)**. *Cellulose* 2021, **28**(7):4089-4103.
53. Matebie BY, Tizazu BZ, Kadhem AA, Venkatesa Prabhu S: **Synthesis of Cellulose Nanocrystals (CNCs) from Brewer's Spent Grain Using Acid Hydrolysis: Characterization and Optimization**. *Journal of Nanomaterials* 2021, **2021**(1):7133154.
54. Starink MJ: **The determination of activation energy from linear heating rate experiments: a comparison of the accuracy of isoconversion methods**. *Thermochim Acta* 2003, **404**(1):163-176.
55. Sbirrazzuoli N, Vincent L, Mija A, Guigo N: **Integral, differential and advanced isoconversional methods: Complex mechanisms and isothermal predicted conversion–time curves**. *Chemometrics and Intelligent Laboratory Systems* 2009, **96**(2):219-226.
56. Barud HS, Ribeiro CA, Capela JM, Crespi MS, Ribeiro SJ, Messadeq Y: **Kinetic parameters for thermal decomposition of microcrystalline, vegetal, and bacterial cellulose**. *J Therm Anal Calorim* 2011, **105**(2):421-426.
57. Badran I, Thaher MN: **Isoconversional and DFT Investigation of the Thermal Decomposition of Levofloxacin**. *Moroccan Journal of Chemistry* 2025, **13**(1):248-268.
58. Fang M, Ivanisevic J, Benton HP, Johnson CH, Patti GJ, Hoang LT, Uritboonthai W, Kurczy ME, Siuzdak G: **Thermal Degradation of Small Molecules: A Global Metabolomic Investigation**. *Anal Chem* 2015, **87**(21):10935-10941.
59. Borucka M, Celiński M, Sałasińska K, Gajek A: **Identification of volatile and semi-volatile organic compounds emitted during thermal degradation and combustion of triadimenol**. *J Therm Anal Calorim* 2020, **139**(2):1493-1506.
60. Carrión-Prieto P, Martín-Ramos P, Hernández-Navarro S, Sánchez-Sastre LF, Marcos-Robles JL, Martín-Gil J: **Crystallinity of cellulose microfibers derived from Cistus ladanifer and Erica arborea shrubs**. *Maderas Ciencia y tecnología* 2019, **21**(4):447-456.